G. MANDAL[1], S.K. GHOSH[1*], S. CHATTERJEE[1]

EFFECT OF THERMOMECHANICAL CONTROLLED PROCESSING AND QUENCHING & TEMPERING ON THE STRUCTURE AND PROPERTIES OF BAINITE-MARTENSITE STEELS

In the present time, advanced high strength steel (AHSS) has secured a dominant place in the automobile sector due to its high strength and good toughness along with the reduced weight of car body which results in increased fuel efficiency, controlled emission of greenhouse gases and increased passengers' safety. In the present study, four new advanced high strength steels (AHSS) have been developed using three different processing routes, i.e., thermomechanical controlled processing (TMCP), quenching treatment (Q_T), and quenching & tempering (Q&T) processes, respectively. The current steels have achieved a better combination of the high level of strength with reasonable ductility in case of TMCP as compared to the other processing conditions. The achievable ultrahigh strength is primarily attributed to mixed microstructure comprising lower bainite and lath martensite as well as grain refinement and precipitation hardening.

Keywords: Steels, TMCP, Heat treatment, Microstructure, Mechanical properties

1. Introduction

Since the last few decades in the automotive sector, investigation on the development of advanced high strength steels (AHSS) has been increased with the aim of passenger safety, manufacturing flexibility and recyclability along with eco-friendly benefits [1,2]. These steels have been used in bridges, buildings, pressure vessels, tube, pipelines, vehicles (B-pillar, roof bow, bumper beam etc.), ship hull, submarine hull plate and hydrofoils etc. [3-5]. However, presently, there is an increasing demand for the ultrahigh level of strength in the hot rolled plate as a replacement of heat-treated steel and also to avoid the various defects like quench cracking, distortion or residual stress as well as high production cost owing to heat treatment. It is obvious, that a good combination of mechanical properties of AHSS can be achieved through the proper alloy design followed by various heat treatments, like quenching treatment (Q_T), quenching & tempering (Q&T) and quenching & partitioning (Q&P), etc. [6,7]. However, by controlling rolling schedule and cooling conditions during the thermomechanical process, a superior combination of mechanical properties could be achieved in AHSS plates, like the ultrahigh strength with good ductility and toughness [8]. Such type of thermomechanical process known as thermomechanical controlled processing (TMCP), ensures consistent metallurgical results, cost-effectiveness, productivity and product quality compared to other processing routes (heat treatments) [9]. Alloying elements like Cu, Ni, Mn, Cr and Mo etc. along with microalloying have been utilised in low carbon steel to achieve the ultrahigh strength as well as properties like low-temperature toughness, weldability, ductility and corrosion resistance etc. [10]. In addition, Ni, Mo and Cr have minimised the heterogeneity of microstructure and properties, which have occurred during deformation and different cooling, through the thickness of the as-rolled plate of Ti-Nb microalloyed AHSS steel [11]. The higher amount of Ni gives a high solid solution strengthening as well as improved ductility at low temperatures by lowering the austenite transformation temperature [12]. The multiple microalloying elements such as V, Nb, and Ti have ensured the ultrahigh level of strength by grain refinement and precipitation hardening, as a combination of (Ti + V) or (Ti + Nb) or (Ti + Nb + V) in HSLA steel [13]. The ultrahigh strength of AHSS has been achieved through the grain refinement and precipitation strengthening during the TMCP process [14]. It is earlier reported that heavy deformation is to be the most effective method for grain refinement. However, it is not so easy to give a large amount of deformation on the steel plate by a single pass; as a result, high heat is generated due to ferrite grain growth which attributed to the heavy deformation during rolling [15].

[1] INDIAN INSTITUTE OF ENGINEERING SCIENCE AND TECHNOLOGY, DEPARTMENT OF METALLURGY AND MATERIALS ENGINEERING SHIBPUR, HOWRAH-711103, WEST BENGAL, INDIA

* Corresponding author: skghosh@metal.iiests.ac.in
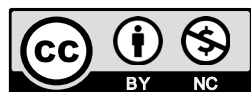
Therefore, a continuous deformation process with a small strain in each pass of deformation has been required in both recrystallisation region ($>T_{NR}$) and non-recrystallisation region ($<T_{NR}$) during TMCP. It is further essential to properly understand the effect of alloy composition and TMCP parameters for achieving the desired properties of as-rolled AHSS steel plate, without any heat treatment, which is scanty in the literature.

Thus, the present investigated steels have been designed with varying carbon (0.08-0.28 wt.%) and co-alloyed with Mn, Ni, Cu and Mo along with Ti and Nb microalloying elements in almost similar levels. Ni and Cu both are commonly used in ultrahigh strength structural steel [16]. Mo is used for increasing hardenability, ultimate tensile strength and creep resistance [16,17]. Subsequently, the cast and forged specimens were separately processed into three routes; the first one is TMCP followed by air cooling (AC) and water quenching (WQ), the second one is hot rolled (HR) followed by Q_T and the third one is hot rolled followed by Q&T process, respectively. Finally, a brief summary has been made in relation to processing, structures and mechanical properties to compare the advancement of TMCP process compared to hot rolling followed by heat treatment processes.

2. Materials and experimental details

The present microalloyed ultrahigh strength steel ingots (250 mm × 50 mm × 50 mm) were made by an air induction furnace of 25 kVA capacity followed by forging into square bars of 16 mm × 16 mm dimension. The forged samples were used for chemical composition (wt.%) analysis and reported in Table 1. Subsequently, the forged specimens were separated into three groups; first one thermomechanical controlled processing (TMCP) followed by air cooling (AC) and water quenching (WQ) process, second one hot rolling (HR) followed by quenching treatment (Q_T) and third one is hot rolling (HR) followed by quenching and tempering treatment (Q&T) process, respectively. A laboratory-scale two-high rolling machine with a roll diameter of 4.5 inches (≈114 mm) was used for both TMCP and HR, respectively. Prior to HR and TMCP, the austenitising temperature (soaking temperature) is maintained at 1200°C for 1h to make homogeneous austenite in forged specimens. All the TMCP samples were allowed to have four-pass thickness reduction schedule in this order: 16 mm → 13 mm → 10 mm → 8 mm → 6 mm (final sheet thickness) at the finish rolling temperature (FRT) of 850°C. In case of TMCP, more than 50% cumulative reduction (summation of total four-pass rolling deformation) has been given below non-recrystallisation temperature (T_{NR}), which is a controlled rolling process. On the other hand, during four-pass hot rolling (HR) process (conventional hot rolling operation, not a controlled rolling operation) 80-90% cumulative amount of deformation has been given above T_{NR} and finally finished at 900°C with 6 mm sheet thickness. Subsequently, all the HR samples were subjected to Q_T and Q&T heat treatment processes, respectively. All the processes were carried out according to the schematic illustration shown in Fig. 1. The non-recrystallisation temperature has been assessed from the chemical composition (wt. %) and applied strain per pass (ε) by the following empirical equations [18,19] which are found to be

TABLE 1

Chemical compositions of the investigated steels (wt.%)

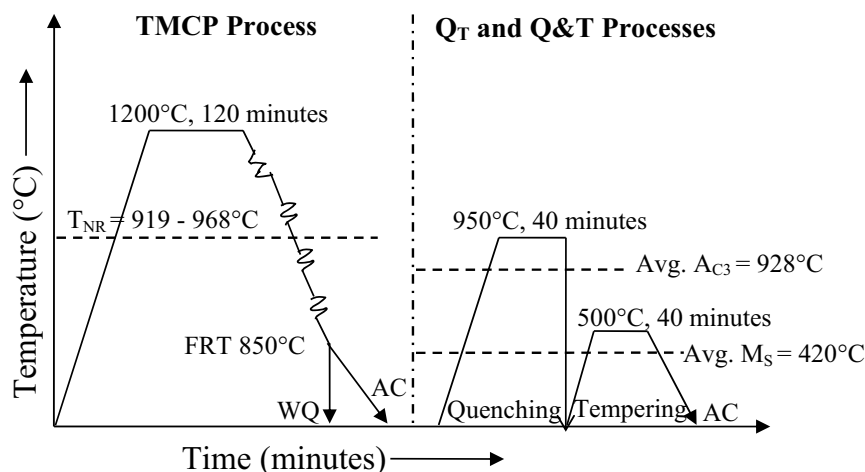| Alloy	C	Mn	Si	Cu	Ni	Mo	Ti	Nb	S	P	N	T_{NR} (°C)
Steel-1	0.08	1.95	0.35	1.71	3.45	1.42	0.06	0.07	0.01	0.01	0.0067	968
Steel-2	0.15	1.90	0.36	—	4.40	1.45	0.06	0.08	0.01	0.01	0.0068	959
Steel-3	0.16	1.96	0.31	1.62	3.27	1.38	0.05	0.07	0.01	0.01	0.0065	945
Steel-4	0.28	1.76	0.35	—	4.40	1.88	0.06	0.08	0.01	0.01	0.0068	919

Fig. 1. Schematic diagram of thermo-mechanical controlled processing (TMCP), quenching treatment (Q_T) and quenching and tempering (Q&T) heat treatment schedule. FRT, T_{NR}, WQ, AC, A_{C3} and M_S stand for finish rolling temperature, Non-recrystallisation temperature, Water quenching, Air cooling, Ferrite to austenite transformation completion temperature during heating and Martensite start temperature, respectively

reliable in the present study.

$$T_{NR} = 203 - 310C - 149\sqrt{V} + 657\sqrt{Nb} + 683e^{-0.36\varepsilon} \quad (1)$$

Where,

$$\varepsilon = \frac{2}{\sqrt{3}} \ln\left(h_i / h_f\right) \quad (2)$$

The estimated average T_{NR} temperatures of these four investigated steels are 968, 959, 945 and 919°C, respectively which are shown in Table 1, considering strain per pass ≈0.28.

All the TMCP and heat-treated samples were characterised through optical microscopy (OM) (Carl Zeiss, Axiovert 40 Mat), high resolution field emission scanning electron microscope (JEOL, JSM-7610F-FESEM) operating at 15-20 kV accelerating voltage in a secondary electron mode after etching of metallographically prepared samples (10 mm × 10 mm) with 2% nital solution and transmission electron microscopy (TEM) (Tecnai, G^2 model at 200 kV) of electron transparent thin samples of about

3 mm diameter and 30-40 μm thickness. The Vickers hardness test was carried out using a universal hardness tester (Innovatest Verzus - 750CCD) with 30 kg load and 20 s dwelling time as per ASTM E92-17 standard [20]. The tensile test was carried out at room temperature of sheet specimens of 25 mm gauge length with an applied strain rate of 3.3×10^{-4} s^{-1} by a 10-ton capacity machine (Instron 8801) using an extensometer as per ASTM E8/E8M-16A standard [21]. The fractographic features of the tensile fractured samples were characterised using a high depth of focus by FESEM in a secondary electron mode.

3. Results and discussion

3.1. Microstructural evolution

All the four newly developed steels have revealed the almost similar type of optical microstructure consisted of bainite
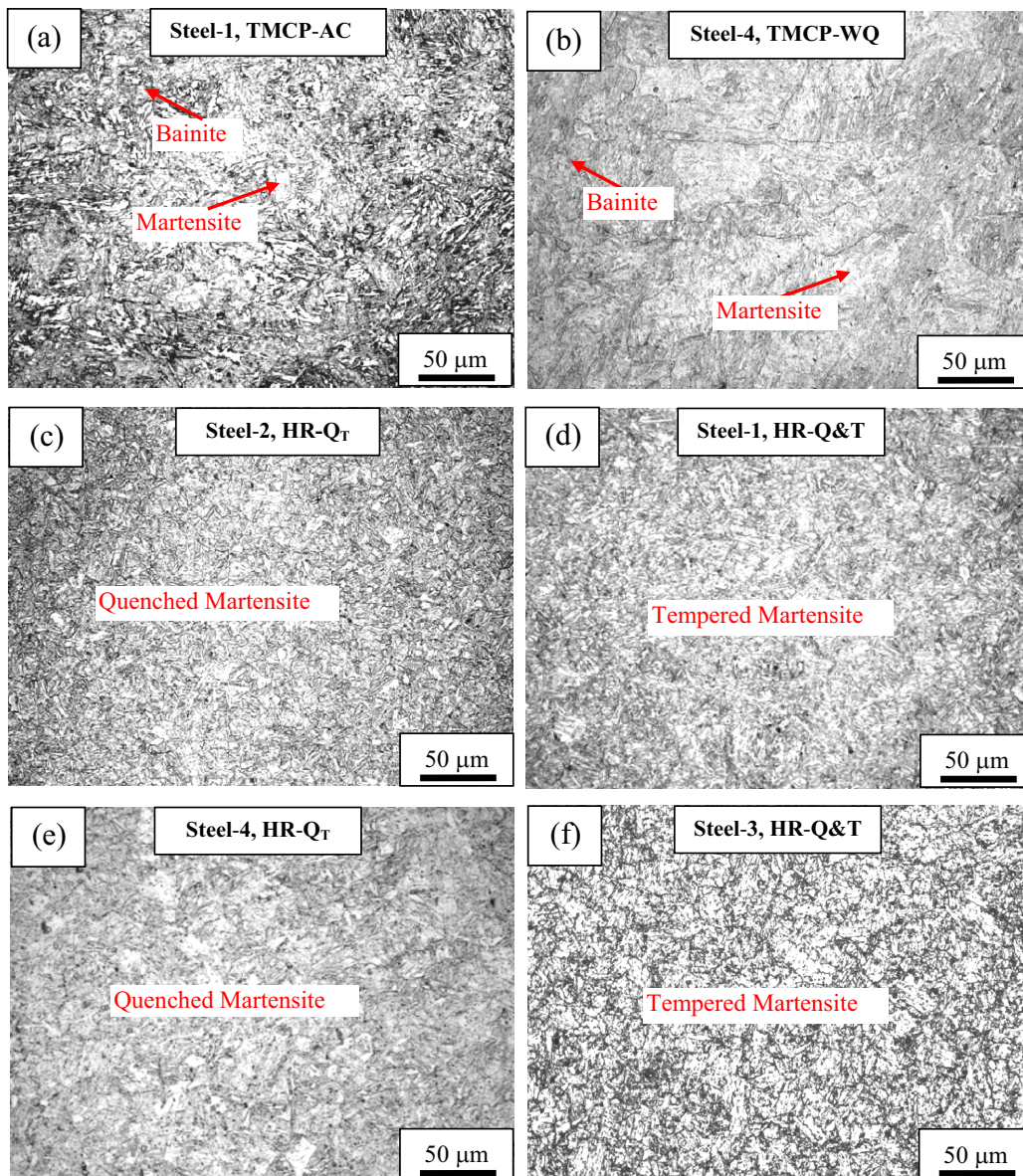

Fig. 2. Some selective optical micrographs of newly developed steels through the various processing conditions

of dark contrast and martensite of bright contrast in case of TMCP followed by both AC and WQ processed specimens, respectively. However, the volume percentages of martensite and bainite have been found in higher amount in water quenched and air cooled samples, respectively and vice versa [1,22,23]. The proper alloy design proposed the higher bainitic hardenability which reflected on the AC sample of all four investigated steels. On the other hand, the WQ samples have exhibited a lower amount of bainite and a higher amount of martensite, because martensite is expected to be of major quantity at the higher cooling rate (WQ). Two selective microstructures of TMCP followed by AC and WQ have been shown in Figs. 2(a) and (b), respectively. All the Q_T and Q&T processed specimens of four steels have exhibited primarily martensite and quenched martensite with tempered martensite, respectively. It is evident that the morphology of quenched martensite and tempered martensite of all experimental steels appear in an almost similar fashion. Some selected micrographs of Q_T and Q&T processed specimens are shown in Figs. 2(c) to (f). It is obvious that microstructure evolution is almost similar comprising bright and dark regions in the all processing condition. However, a careful observation indicates that average microstructural constituent size reduces in the order by following first TMCP-AC, then TMCP-WQ, after that HR-Q&T and finally HR-Q_T sample, respectively.

Fig. 3 shows some selective high-resolution FESEM micrographs of newly developed steels through the various processing conditions which give a better clarity about bainite and martensite characteristics at higher magnification as compared to optical microstructure. Figs. 3(a) and (b) have exhibited a mixed microstructure of bainite and martensite of TMCP followed by AC and WQ of both steels 1 and 2, respectively. On another side, Figs. 3(c) and (d) show the quenched and tempered martensite for HR followed by Q_T and Q&T heat-treated samples of steels 3 and 4, respectively. It is important to note that the lath size of martensite is usually lower (<1 μm) than that of bainite. The presence of carbide as small white dots is evident (Fig. 3(a)) within bainite laths which indicates these as lower bainite phase. During tempering quenched martensite rejects carbon leading to the formation of carbides which are depicted as white dots in high-resolution FESEM micrograph, Fig. 3(d).

The transmission electron microscopy was conducted to examine the fine microstructural constituents which cannot be characterised in FESEM. Figs. 4(a) to (e) show the bright field (BF) electron images of some selective micrographs of the present investigated steels processed at various conditions. Fig. 4(a) of sample processed at TMCP-AC has primarily shown lower bainite along with lath martensite and retained austenite. Some precipitate particles have been formed within bainite plate (Fig. 4(a)) which could be $Ni_3(Ti, Nb)$ or (Nb, Ti)C, contributing high strength through the precipitation hardening [1]. Fig. 4(b) reveals predominantly martensite and lower bainite with high dislocation density as a signature of accommodation strain during phase transformation from austenite to martensite in water quenched TMCP samples. Fig. 4(c) of the sample processed as HR-Q_T demonstrates fine martensite laths (≈100 nm). Fig. 4(d) of the sample processed at HR-Q&T has exhibited tempered martensite laths with intralath and interlath carbides. It is evident that the lath size is finer in case of Q_T than the other processing conditions. Fig. 4(e) shows the three different sized nearly spheri-
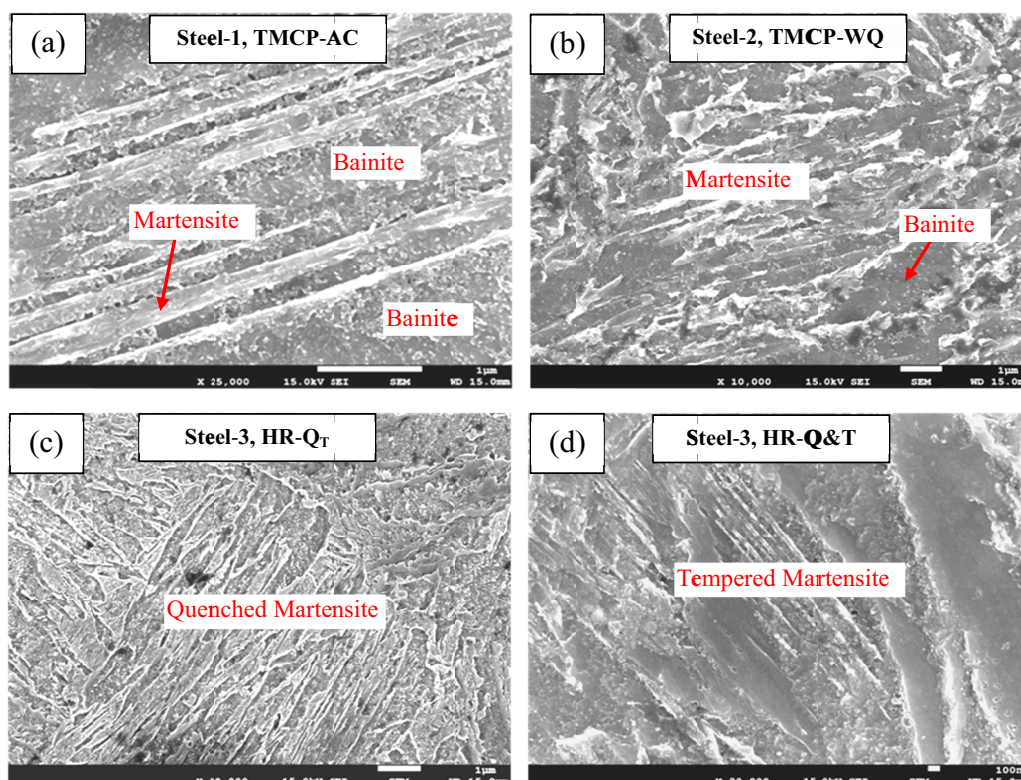

Fig. 3. Some selective FESEM micrographs of newly developed steels through the various processing conditions
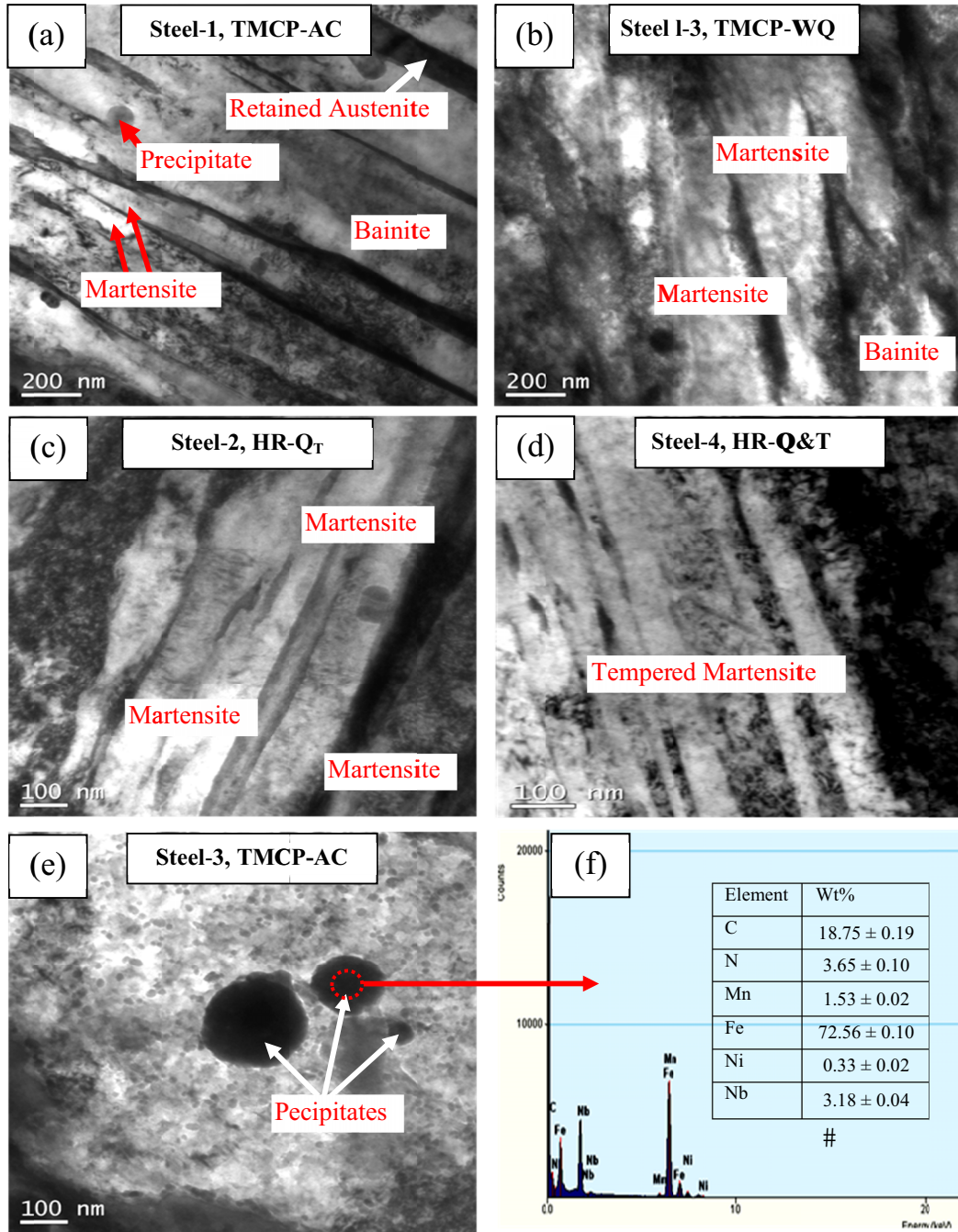
Fig. 4. Some selective bright field TEM micrographs (a)-(e) and (f) EDS analysis of newly developed steels through the various processing conditions

cal precipitates of dark contrast and a lot of very fine precipitates that are uniformly distributed throughout the bainite plate. Those fine precipitates are very much helpful for achieving the ultrahigh level of strength of the present investigated steels by the means of dislocation-precipitate interaction during experimental rolling operation [24]. On the other hand, Fig. 4(f) shows the EDS spectrum of red circled precipitate (denoted by arrow) and the corresponding analysis results have confirmed the presence of NbC/NbCN in that steel.

It is well known that Nb influences microstructures and mechanical properties through solid solution during homogenisation before controlled rolling [25]. As the deformation continues with the rolling process and decrease of temperature, supersatu-

rated Nb precipitates out from the solution to form NbC at grain boundaries and dislocations [26]. It is a fact that both solute drag of Nb in solid solution and pinning of NbC particles restrain the grain boundary during grain growth after recrystallisation in low carbon Nb-microalloyed steels [27]. In the traditional hot rolling or austenitising temperature range, a strong suppression for grain growth after recrystallisation could be obtained due to fine NbC particles smaller than 10 nm in Nb-microalloyed steels [28,29]. The numerous fine carbides of Nb and Ti led to remarkable precipitation strengthening effect [30,31] in the present steel. Thus, the strength and toughness of the present steels are improved by the combination of grain refinement and precipitation strengthening mechanisms.

It is logical that the separation of bainite and martensite phase in Fig. 4 is very difficult without selected area electron diffraction (SAED) pattern. However, in the absence of SAED, the aforesaid two phases have been distinguished from the width dimension, carbide precipitate and dislocation density of the lath constituents of the microstructure which is in agreement with the earlier study [31]. The finer lath along with high dislocation density and no carbide precipitation indicate the martensite lath. Whereas, the wider lath having carbide precipitate and relatively low dislocation density denote bainite lath. The interlath thin film-like black layers show typically retained austenite which is also expected due to high nickel content in the present steels.

3.2. Mechanical properties and fractographic features

Table 2 shows the mechanical properties i.e., hardness and tensile properties of the newly developed four investigated steels. It is evident that the water quenched samples after TMCP has exhibited the best combination of mechanical properties compared to other processing routes, irrespective of the investigated steels (alloys). Although the TMCP-AC sample shows a little bit of higher value of total elongation (TEL) compared to WQ samples, the hardness, yield strength (YS) and ultimate tensile strength (UTS) values are higher in case of WQ samples. All the quenching treated (Q_T) specimens show an almost similar type of properties of TMCP-WQ irrespective of alloys. In addition, quenching and tempering (Q&T) processed samples show the lower value of all hardness, YS and UTS compared to quenching treated (Q_T) specimen but the total elongation value is higher due to the tempering of martensite. All the TMCP processed samples have shown the higher value of tensile toughness (TT) compared to HR followed by Q_T and

Q&T heat-treated specimens irrespective of steel type, which is attributed to more grain refinement during TMCP. Actually, tensile toughness is expressed as the area under the tensile stress-strain curve which is the product of stress and strain. Strain having no unit, the toughness is expressed in the unit of stress i.e., MPa. The higher hardness, UTS and lower YS have been achieved in case of TMCP-WQ and Q_T processed specimens than those of TMCP-AC and Q&T specimens due to a higher amount of martensite formation during quenching. On the other hand, TMCP-AC and Q&T processed specimens show the higher total elongation compared to other specimens possibly due to the mixed microstructure of bainite-martensite and tempered martensite, respectively. The samples processed with TMCP reveal higher strength, ductility and toughness which is attributed to grain/lath refinement during TMCP [23].

Fig. 5 shows some selective high-resolution FESEM micrographs of tensile fracture surfaces of newly developed steels through the various processing conditions which give a better insight about the nature of tensile fracture and its various characteristics. It is evident that all tensile fracture surfaces of all steels have exhibited a mixed-mode of the fracture i.e., ductile and brittle comprising cleavage facets, ductile tearing, micro-voids, shear lip, dimples with some intergranular cracks indicating a considerable amount of deformation before fracture. Fig. 5(a) shows cleavage facets and ductile tearing which give more ductility compared to TMCP-WQ sample (Fig. 5(b)), where micro-voids and shear lips are dominant. On the other hand, in Fig. 5(d), the presence of fine dimple indicates higher ductility as compared to that of water quenched sample having intergranular crack denoted by an arrow on the fracture surface, Fig. 5(c). Thus, the fractographic features have substantiated the tensile results of the investigated high strength steels.

From the above results and discussion, it can be highlighted that the present investigated ultrahigh strength steels

TABLE 2

Hardness and tensile properties under the various processing conditions

| Steels	Processing conditions	Hardness (HV)	Yield Strength (MPa)	Tensile Strength (MPa)	Total Elongation (%)	Tensile Toughness (MPa)
Steel-1	TMCP-AC	351±4	990±6	1438±7	13±1	110±5
	TMCP-WQ	385±5	1183±9	1503±9	11±1	100±7
	HR-Q_T	375±4	1150±8	1308±8	10±1	92±6
	HR-Q&T	365±4	1080±8	1270±7	13±1	99±6
Steel-2	TMCP-AC	442±5	1102±8	1641±7	13±1	116±5
	TMCP-WQ	487±4	1410±9	1712±8	10±1	109±7
	HR-Q_T	471±6	1385±9	1590±9	9±1	93±5
	HR-Q&T	458±6	1280±8	1379±9	12±1	102±6
Steel-3	TMCP-AC	361±5	1025±7	1583±7	12±1	110±7
	TMCP-WQ	440±5	1216±7	1718±8	11±1	101±5
	HR-Q_T	451±4	1218±8	1495±7	9±1	91±4
	HR-Q&T	445±4	1108±7	1450±7	11±1	98±5
Steel-4	TMCP-AC	480±5	1458±9	1838±8	8±1	90±4
	TMCP-WQ	475±6	1431±9	1982±9	6±1	82±6
	HR-Q_T	482±5	1406±8	1807±9	7±1	79±4
	HR-Q&T	470±4	1368±9	1723±8	9±1	81±4
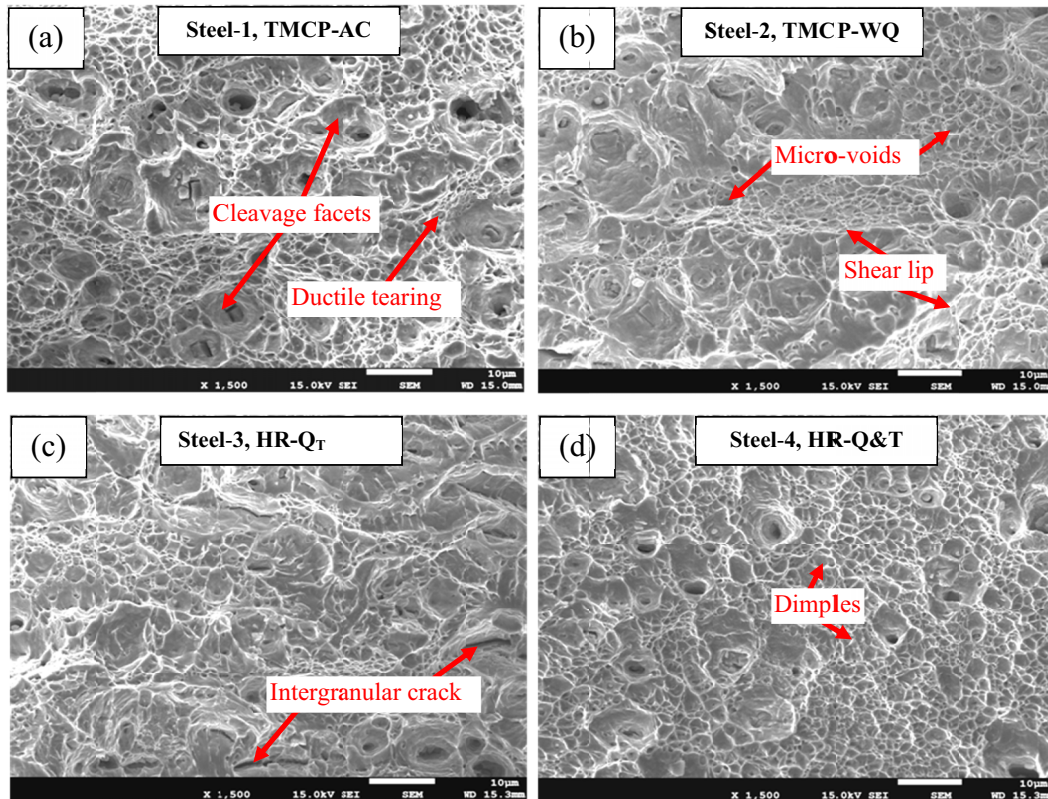
Fig. 5. Some selective FESEM micrographs of fracture surfaces of newly developed steels

can be thermomechanically processed in the industry to develop a suitable combination of bainite-martensite microstructure and mechanical properties. These developed steels can be potential candidates in automobile, structural and safety-related applications. The mechanical properties achieved therein are equivalent to various industrial steel grades such as Docol 1400 [32], AISI 4340 [33], JIS SNCM 439 [34], JIS SNCM 440 [34], tribond® 1400 [35] etc.

4. Conclusions

In the present study, four low to medium carbon microalloyed ultrahigh strength steels have been developed through TMCP, Q_T and Q&T processes for achieving attractive mechanical properties. The major conclusions are listed below.

1. All the investigated steels have exhibited an almost similar type of microstructural constituents with bainite and martensite. However, TMCP-AC processed samples have revealed the larger amount of bainite than TMCP-WQ sample and the lath size becomes finer ($\approx$100 nm) in case of WQ and Q_T samples compared to the other processing routes.
2. TMCP-WQ sample has shown the maximum UTS (1503-1982 MPa) due to the presence of adequate finer quenched martensite.
3. Microalloying elements (Ti, Nb) have played a dominant role to develop an ultrahigh level of strength through the grain refinement and precipitation strengthening.
4. A reasonably good amount of ductility (6-13%) of the present investigated steels has been manifested by the mixed-mode (ductile and brittle) of fracture surface morphology.
5. The newly designed TMCP schedule has offered a better combination of mechanical properties as compared to other heat treatment processes (Q_T and Q&T) and it will be cost-effective for industrial-scale production.

REFERENCES

[1] G. Mandal, S.K. Ghosh, D. Chakrabarti, S. Chatterjee, Metallography, Microstructure and Analysis **7**, 222-238 (2018).
[2] M.St. Węglowski, M. Zeman, A. Grocholewski, Archives of Metallurgy and Materials **61** (1), 127-132 (2016).
[3] S.K. Ghosh, P.S. Bandyopadhyay, S. Kundu, S. Chatterjee, Materials Science and Engineering A **528**, 7887-7894 (2011).
[4] D.S. Liu, B.G. Cheng, Y.Y. Chen, Metallurgical and Materials Transactions A **1**, 440-455 (2013).
[5] J. Hu, L.X. Du, H. Liu, Materials Science and Engineering A **647**, 144-151 (2015).
[6] D.K. Matlock, J.G. Speer, Materials and Manufacturing Processes **25**, 7-13 (2010).
[7] L. Kučerová, H. Jirková, B. Mašek, Archives of Metallurgy and Materials **59** (3), 1189-1192 (2014).
[8] A. Grajcar, P. Skrzypczyk, R. Kuziak, K. Golombek, Steel Research International **85**, 1058-1069 (2014).
[9] R. Ranjan, H. Beladi, S.B. Singh, P.D. Hodgson, Metallurgical and Materials Transactions A **46A**, 3232-3247 (2015).

868

[10] B.E. Keehan, L. Karlsson, H.O. Andren, H.K.D.H. Bhadeshia, Welding **85**, 200-210 (2006).

[11] Z.Q. Cao, Y.P. Bao, Z.H. Xia, International Journal of Minerals, Metallurgy, and Materials **5**, 567-572 (2010).

[12] S. Zhang, P. Wang, D. Li, Y. Li, Materials and Design **84**, 385-394 (2015).

[13] A.J. Craven, K. He, L.A.J. Garvie, T.N. Baker, Acta Materialia **48**, 3857-3868 (2000).

[14] C.-N. Li, X.-L. Li, G. Yuan, R.D.K. Misra, J. Kang, G.-D. Wang, Materials Science and Engineering A **673**, 213-221 (2016).

[15] Y.H. Bae, J.S. Lee, J.-K. Choi, W.-Y. Choo, S.H. Hong, Materials Transactions **45** (1), 137-142 (2004).

[16] E. Lichańska, M. Sułowski, A. Ciaś, Archives of Metallurgy and Materials **61** (1), 109-114 (2016).

[17] K. Prusik, E. Matyja, M. Wąsik, M. Zubko, Archives of Metallurgy and Materials **64** (2), 733-738 (2019).

[18] F. Fletcher, Meta-analysis of T_{NR} measurements: determining new empirical models based on composition and strain, in: Austenite Processing Symposium (Internal company presentation), 1-14 (2008).

[19] C. Ma, L. Hou, J. Zhang, L. Zhuang, Materials Science and Engineering A **650**, 454-468 (2016).

[20] Standard Test Methods for Vickers Hardness and Knoop Hardness of Metallic Materials: ASTM E92- 17, (2017). DOI: 10.1520/E0092-17.

[21] Standard Test Methods for Tension Testing of Metallic Materials: ASTM E8/E8M-16A, (2016). DOI: 10.1520/E0008_E0008M-16A.

[22] G. Mandal, S.K. Ghosh, D. Chakrabarti, S. Chatterjee, Journal of Materials Engineering and Performance **27** (12), 6516-6528 (2018).

[23] G. Mandal, C. Roy, S.K. Ghosh, S. Chatterjee, Journal of Alloys and Compounds **705**, 817-827 (2017).

[24] K. Bolanowski, Archives of Metallurgy and Materials **61** (2), 475-480 (2016).

[25] H. Wu, B. Ju, D. Tang, R. Hu, A. Guo, Q. Kang, D. Wang, Materials Science and Engineering A **622**, 61-66 (2015).

[26] D.H. Jack, K.H. Jack, Materials Science and Engineering **11**, 1-27 (1973).

[27] L. Fu, A. Shan, W. Wang, Acta Metallurgica Sinica **46**, 832-837 (2010).

[28] A. Sarkar, S. Sanyal, T.K. Bandyopadhyay, S. Mandal, Materials Science and Engineering A **703**, 205-213 (2017).

[29] H. Pan, H. Ding, M. Cai, D. Kibaroglu, Y. Mab, W. Song, Materials Science and Engineering A **766**, 138371 (2019).

[30] N. Zhong, X.D. Wang, L. Wang, Y.H. Rong, Materials Science and Engineering A **506**, 111-116 (2009).

[31] W. Xiong, R. Song, P. Yu, W. Huo, S. Qin, Z. Liu, Steel Research International, **1900224**, 1-10 (2019) DOI: 10.1002/srin.201900224.

[32] J.O. Sperl K. e,Olsson, High strength and ultra-high strength steels for weight reduction in structural and safety-related applications, Proceedings of ISATA 29th International Symposium on Automotive Technology and Automation, Florence, **I**, 115-125 (1996).

[33] W.-S. Lee, T.-T. Su, Journal of Materials Processing Technology **87** (1-3), 198-206 (1999).

[34] D.Y. Wei, J.L. Gu, H.S. Fang, B.Z. Bai, Z.G. Yang, International Journal of Fatigue **26** (4), 437-442 (2004).

[35] ThyssenKrupp, Steel, Product information tribond®, **2**, 1-10 (2016).